α-γ transition in metallic Ce studied by resonant x-ray spectroscopies

C. Dallera,[1] M. Grioni,[2] A. Palenzona,[3] M. Taguchi,[4] E. Annese,[5] G. Ghiringhelli,[1] A. Tagliaferri,[1] N. B. Brookes,[6] Th. Neisius,[6] and L. Braicovich[1]

[1]*INFM–Dipartimento di Fisica, Politecnico di Milano, piazza Leonardo da Vinci 32, 20133 Milano, Italy*
[2]*IPN, Ecole Polytechnique Fédérale, CH-1015 Lausanne, Switzerland*
[3]*INFM–Università degli Studi, Dipartimento di Chimica e Chimica Industriale, via Dodecaneso 31, I-16146 Genova, Italy*
[4]*RIKEN/Spring-8, 1-1-1, Mikazuki-cho, Sayo-gun, Hyogo 679-5148, Japan*
[5]*INFM–Dipartimento di Fisica, Università di Modena e Reggio Emilia, via Campi 213/A, I-41100 Modena, Italy*
[6]*European Synchrotron Radiation Facility, BP 220, F-38043 Grenoble, France*

We performed bulk-sensitive x-ray absorption (XAS) in the partial fluorescence yield (PFY) mode, and resonant x-ray emission (RXES) measurements of the solid solution Sc (7 at.%):Ce at the Ce L_3 $(2p \rightarrow 5d)$ and $M_{4,5}$ $(3d \rightarrow 4f)$ absorption edges. We deduce an increasing $4f$-band hybridization from the γ-phase stable at room temperature to the low-temperature α-Ce, consistent with the "Kondo collapse" scenario for the transition. The enhanced intrinsic resolution of PFY-XAS allows us to resolve the elusive three-peak structure predicted by theory. Thanks to the selective enhancement typical of RXES, we could estimate the small but non-negligible contribution of the f^2 configuration in the hybrid ground state, and its change in the two phases. The linear dichroism effect in the $M_{4,5}$ RXES spectra is consistent with the observed hybridization of $4f$ and conduction states.

I. INTRODUCTION

Cerium, with its compounds, plays the role of a model system to investigate the effects of strong electronic correlations, including intermediate valence and unusual magnetic and transport properties. Conventional band theory, based on independent particles and extended wavefunctions, is not well adapted to tackle this problem.[1] A local approach based on the Anderson impurity model (AIM) gives a better description of the strong Coulomb interactions, and the delicate balance between localization and delocalization which is at the origin of the "Kondo" behavior.[2]

Metallic cerium presents a further element of interest. As a function of temperature or pressure it undergoes a unique first-order isostructural (fcc $\rightarrow$ fcc) phase transition from the γ-phase, stable at ambient conditions, to a low-temperature (or high-pressure) α-phase, with a loss of magnetic moments and a huge (15%) volume reduction.[3] This was initially interpreted as a result of the sudden promotion of the $4f$ electron to the conduction band,[4] but various experiments have ruled out the large changes in the $4f$ occupation required by that model. Johansson[5] suggested that the $4f$ electrons are localized in γ-Ce, but form a narrow band in α-Ce, so that the transition should be considered a Mott transition. According to the now prevailing "Kondo collapse" scenario[6] based on the AIM, the $4f$ states are partially localized in both phases, but the $4f$ occupation varies between $n_f \sim 0.95$ (γ-Ce) and $n_f \sim 0.85$ (α-Ce), resulting in quite different properties. The relevant parameters for the transition are the Kondo (i.e., spin-fluctuation) energy and entropy, rather than the much larger energy associated with charge fluctuations as implied by the Mott transition model. In γ-Ce the $4f$-band hybridization is small, and the characteristic Kondo temperature $T_K(\gamma$–Ce$) \sim 20$ K is much lower than

that of the strongly-hybridized α-phase $[T_K(\alpha$-Ce$) \sim 1000$ K]. Two opposite situations, $T/T_K(\alpha$-Ce$) \ll 1$ and $T/T_K(\gamma$-Ce$) \gg 1$, can therefore be realized in the two phases.

The Mott and "Kondo collapse" models have usually been regarded as mutually exclusive, but numerical results of the dynamical mean-field theory (DMFT) have recently revealed unsuspected analogies between the two scenarios.[7,8] High-energy spectroscopies have contributed to establishing the Kondo scenario for Ce systems, and provided direct estimates of the free parameters of the AIM.[9,10] Their ability to measure both large (charge fluctuation) and small (Kondo) energy scales is an advantage over the thermodynamic or magnetic probes. Valence band photoemission (PES, XPS), inverse photoemission, and core-level XPS data on Ce-based materials reveal an impressive qualitative, and sometimes quantitative agreement, with the calculated spectral properties of the AIM.[11,12]

In spite of this success, the large surface sensitivity of electron spectroscopies is a serious limitation when studying strongly correlated materials, and particularly intermediate-valence compounds. The different atomic environment and lattice parameters often conspire to reduce hybridization and screening at the surface. Since the nature of the ground state is very sensitive to these parameters, the surface and bulk electronic properties in Ce-based materials may be rather different. The surface is usually characterized by reduced—sometimes even strongly reduced—Kondo temperatures, and by n_f values closer to 1.[13–15] This has provoked arguments on the relevance of the AIM for real materials.[16] There is therefore considerable interest for photon in–photon out spectroscopies which are intrinsically bulk sensitive. With the advent of 3rd generation sources of synchrotron radiation, established spectroscopies like x-ray absorption (XAS) have been improved, and novel probes of strongly correlated ma-

terials like resonant x-ray emission (RXES) have emerged.[17–19] RXES was recently used for probing the degree of localization of the $4f$ electrons for CeO_2.[20] In particular, linear dichroism effects in $M_{4,5}$ RXES were predicted and experimentally confirmed[21–23] to bear fingerprints of the ground state symmetry.

We have revisited the classic problem of the Ce α-γ transition by XAS and RXES measurements at the Ce L_3 ($2p_{3/2}$) and $M_{4,5}$ ($3d$) edges. The results confirm the sensitivity of both techniques to the bulk ground state properties, and the ability of RXES to selectively enhance the contribution of specific electronic configurations by an appropriate choice of the excitation energy. These data also yield new elements for the interpretation of the spectral properties of Ce compounds. Namely, we could unambiguously identify in the L_3 XAS spectrum the fingerprint of the f^2 ground state component, predicted by theory, but never established by experiment.

II. EXPERIMENTAL

Samples (about 3 g. each) of the Sc (7:at.%): Ce solid solution were prepared by melting in an induction furnace chips of the two metals well mixed and pressed together. They were then annealed at 500 °C for 10 days. All manipulations were carried out in a glove-box under an atmosphere purified up to 1 ppm of H_2O and O_2. At atmospheric pressure pure Ce transforms below RT to a low-T_K dhcp phase (β-Ce) which only partially transforms to α-Ce at a lower temperature ($\sim$100 K). The addition of 7 at.% Sc prevents the formation of β-Ce, with minor effects on the temperature, sharpness and volume jump of the α-γ transition.[24] Samples for the hard- and soft x-ray measurements were mounted on He cryostats, where the temperature could be varied between 20 K and 300 K.

We performed XAS and RXES measurements at the ESRF (Grenoble). Ce L_3 ($h\nu$=5723 eV) XAS data were obtained at beamline ID26. X-rays from the undulator source were monochromatized by a Si(220) double-crystal monochromator and focused to a 0.3×1.0 mm^2 spot size (H $\times$ V). The sample was polished in air, and then inserted in a high-vacuum system (p=10^{-7} mbar), equipped with 25 μm thick kapton windows for the incident and emitted x-ray beams. Total fluorescence yield (TFY) XAS spectra were collected by a Si diode. For partial fluorescence yield (PFY) XAS and RXES measurements, the scattered beam was monochromatized by a spherically bent (R=1 m) Si(400) analyzer. The scattering angle was 90° to minimize Thomson scattering, and the overall energy resolution was better than 1.5 eV. For the Ce $M_{4,5}$ ($h\nu$=882,900 eV) XAS and RXES we utilized the ID8 soft x-ray beamline, whose APPLE II type undulator provides full polarization control. The sample was scraped in UHV by a diamond file. For the XAS experiment the incident beam was monochromatized by the high-resolution (ΔE=250 meV) Dragon monochromator, and spectra were measured simultaneously in the total electron yield (TEY) and total fluorescence yield (TFY) modes. RXES data were measured using the AXES spectrometer[25] equipped with a CCD camera detector, and its dedicated
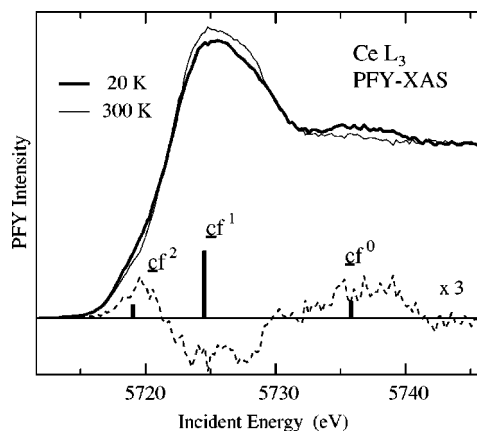

FIG. 1. Ce L_3 PFY-XAS spectra of Sc:Ce in the γ (T=300 K) and α (T=20 K) phases, and difference spectrum (20 K–300 K). The bar diagram schematically represents the relative energies and intensities of the $3d^9 4f^N$ final states, from $3d$ XPS data.

monochromator, with a combined resolution of 0.8 eV.[26] Incidence and emission angles were 10° grazing and 10° from normal, respectively, to minimize self-absorption of the scattered beam.

III. RESULTS AND DISCUSSION

A. XAS

High-resolution Ce L_3 PFY-XAS spectra (Fig. 1) were measured by recording, as a function of incident energy, the intensity of the characteristic Ce $L\alpha_1$ fluorescence ($h\nu$ =4840 eV), emitted after the L_3 absorption according to $|\Psi_0\rangle \rightarrow 2p^5 4f^N k \rightarrow 2p^6 3d^9 4f^N k$. Here $|\Psi_0\rangle$ is the hybrid ground state of a Ce ion, and k is a conduction electron of d (or s) symmetry, as required by dipole selection rules. When the emitted photons are collected within a narrow energy window—in the PFY mode—spectral features are narrower than in conventional total (electron or photon) yield measurements.[27] Qualitatively, the normal L_3 XAS reflects the lifetime broadening (ΔE $\sim$ 4–5 eV) of the deep $2p$ core hole in the final state, while the more complex PFY-XAS only feels the smaller broadening (ΔE $\sim$ 0.4 eV) of the shallower $3d$ hole.[28] It was later realized[29–31] that in general a PFY-XAS spectrum is not strictly equivalent to XAS with reduced broadening, because many-body effects may be different in the final states of the two processes. Nevertheless, the higher spectral definition is of great value and features that are hidden in the broad XAS spectrum may become visible in PFY-XAS thanks to the sharper lineshape.

Even if the $4f$ electrons are "spectators" in the L_3 absorption process, XAS final states with different $4f$ configurations have different energies due to the $4f$–$4f$ and $2p$–$4f$ Coulomb interactions.[9] The main peak at 5725 eV has mostly $\underline{c}f^1$ character (hereafter, $\underline{c}$ stands for a $2p$ or $3d$ core hole), while the satellite at $\sim$11 eV higher energy has almost pure $\underline{c}f^0$ character. It is common practice to extract the Ce valence from the ratio of the intensities of these two features. This procedure has been questioned, but the relative intensity is a useful qualitative indicator of valence.[32,33] The decrease
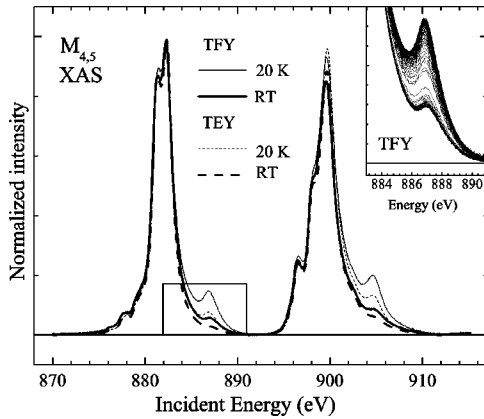
FIG. 2. TFY and TEY $M_{4,5}$ XAS spectra of Sc:Ce at 20 K (α phase) and 300 K (γ phase). The inset shows temperature-dependent changes of the M_5 f^1 satellite at 887 eV as measured by TFY.
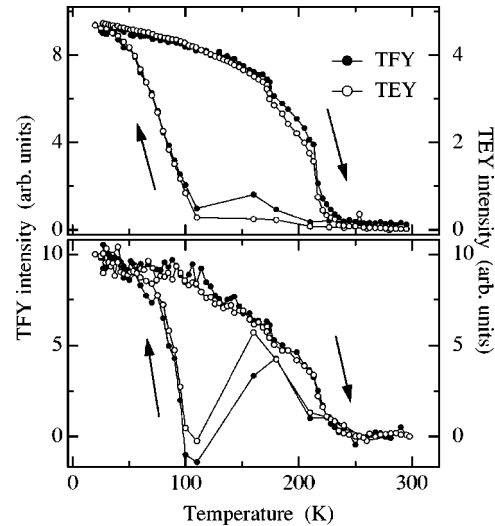

FIG. 3. Evolution of the intensities of the M_5 f^1 satellite (top) and of the main peak of the M_4 spectrum (bottom) for a complete 300 K–20 K–300 K cycle. Irregularities in the intensity trend during the cooling phase (around 170 K) are related to temperature instabilities.

of the main peak and corresponding increase of the satellite at low temperature is consistent with published data.[34] It reflects larger hybridization and smaller n_f in the α phase, as confirmed by a model calculation (see below).

Both spectra exhibit a third weaker feature, clearly visible in the difference spectrum, ~5 eV below the main peak. This feature is predicted by AIM calculations, and the lack of experimental confirmation was puzzling. It was pointed out[32] that the Coulomb interaction between the 4f and the (localized) extra 5d electron in the final state would increase the energy of the $\underline{c}f^2$ feature, which could therefore merge with the main peak. Indeed, three separate peaks are observed in Ce 3d XPS spectra, where no extra 5d electron is present. However, this interaction, which is certainly large (4–5 eV) in insulators like CeO_2,[32] should be considerably reduced by screening in metallic materials. The high-resolution PFY data of Fig. 1 prove that only the large lifetime broadening of the 2p hole prevents observation of a separate $\underline{c}f^2$ feature in conventional L_3 XAS measurements. From the close correspondence with the 3d XPS spectrum[35] (bars) we can also conclude that screening of the 4f–5d Coulomb interaction in Ce must be small, probably below 1 eV.

The $M_{4,5}$ (3d→4f) TFY and TEY XAS spectra of Fig. 2 are dominated by those states of the spin-orbit split $3d^9 4f^2$ multiplet that can be reached via a dipole transition from the $4f^1$ component of the ground state.[36] Valence mixing in the ground state is revealed by the $\underline{c}f^1$ satellites at 887 eV and 905 eV. Neglecting the small hybridization in the final state,[11] their intensities reflect the weight of the f^0 component in the initial state. At RT, in the γ-phase, the TFY spectrum is consistent with $n_f \sim 1$. At 20 K a large increase of the satellite intensity, and a decrease of the M_5/M_4 branching ratio are observed. The satellites are consistently weaker in the more surface-sensitive TEY spectra, suggesting a weaker hybridization of the surface layer. The inset to Fig. 2 shows the increase of the satellite intensity in the TFY spectra with decreasing temperature.

We have followed the evolution of the $M_{4,5}$ spectrum over a complete cycle 300 K→20 K→300 K. The cooling/heating rate was ~2 K/min. Figure 3 shows the temperature

dependence of the intensities of the f^1 satellite at 887 eV (top) and of the maximum of the M_4 multiplet at 900 eV (bottom). They were extracted from the experimental TFY and TEY spectra, after normalization to the incident beam intensity and, for the satellite, subtraction of the 300 K spectrum as a reference. A rapid increase of the satellite signal at ~100 K on cooling marks the onset of the phase transition. Both signals exhibit a similar temperature dependence and a large hysteresis. It is clear from Fig. 3 that the intensity of the M_4 peak is also a good spectroscopic indicator of the 4f configuration. The link between the M_5/M_4 intensity ratio and ground state configuration has been discussed within the AIM in Ref. 38. A weakly hybridized ($n_f \sim 1$) Ce impurity has an almost pure $4f_{5/2}$ ground state, but in the nonspherically symmetric environment of a solid, both $4f^0$ and $4f_{7/2}^1$ configurations are allowed to mix, and their weight increases with increasing 4f-band hybridization. The energy distribution of the $M_{4,5}$ multiplets from $4f_{5/2}$ and $4f_{7/2}$ initial states is different, and the overall M_4/M_5 branching ratio reflects—indirectly—the strength of hybridization and of configuration mixing in the ground state, as shown in Figs. 2 and 3.

B. RXES

The Ce $L\alpha_1$ RXES spectra of Fig. 4, measured along the Ce L_3 XAS profile (excitation energies are shown by dots in the inset), correspond to a radiative decay which leaves a Ce $3d_{5/2}$ hole in the final state: $2p^6 4f^N \rightarrow 2p^5 4f^N k \rightarrow 2p^6 3d^9 4f^N k$. At resonance, absorption and emission occur in a second-order optical process, and the cross-section is expressed by the Kramers-Heisenberg formula.[37] As for L_3 XAS or 3d XPS, the Ce 4f electrons are "spectators," but the 4f–4f and 3d–4f Coulomb interactions give rise to structure in the spectrum. The spectra are plotted as a function of the energy transferred to the solid in the inelastic scattering process: $h\nu_T = h\nu_{IN} - h\nu_{OUT}$.
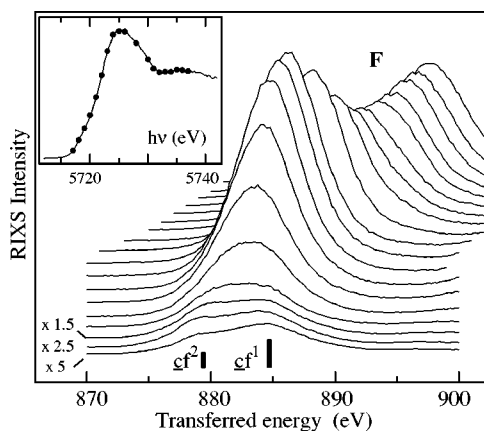
FIG. 4. Lα RXES spectra of Sc:Ce measured at 20 K between $h\nu_{IN}$=5717 (bottom) and $h\nu_{IN}$=5737 (top) along the L$_3$ XAS profile (excitation energies are shown by the dots in the inset). The vertical bars indicate the energies of the $\underline{c}f^2$ and $\underline{c}f^1$ configurations, measured by $3d$ XPS. The dispersing peak (F) is the normal Ce Lα1 fluorescence.

Two features at 880 eV and 885 eV exhibit Raman behavior (constant $h\nu_T$) over a range of incident energies of several eV's, while their intensities are separately enhanced at their respective resonances. At higher incident energies, outside the Raman regime, the dispersing—in the representation of Fig. 4—Ce Lα fluorescence (F) dominates the spectra. As noticed in a previous RXES experiment on Ce-based materials,[39] the energies of the two "Raman" features coincide with the energies of the $3d^9 4f^2$ and $3d^9 4f^1$ configurations, as measured by Ce $3d$ XPS. Accordingly, their intensities are largest when the excitation energy coincides, respectively, with the $2p^5 4f^2$ and $2p^5 4f^1$ features of the L$_3$ XAS spectrum (Fig. 1). The intense fluorescence masks the RXES signature of the $2p^5 4f^0$ final state configuration, expected at $\sim$895 eV.

The peak at 880 eV transferred energy has been observed in RXES data on CeF$_3$,[39] and initially assigned to a quadrupolar (E2) $2p^6 4f^1 \rightarrow 2p^5 4f^2 \rightarrow 2p^6 3d^9 4f^2$ transition. This was not confirmed by experiments on related lanthaum compounds,[40] where the same authors demonstrated by a detailed analysis that pre-edge signal is predominantly associated with dipole (E1) transitions. The dipolar origin of this feature is further supported by a semiquantitative analysis (Fig. 5) of the spectrum measured in correspondence of the $\underline{c}4f^2$ XAS structure ($h\nu_{IN}$=5719 eV). For the $\underline{c}f^2$ component we arbitrarily chose a Gaussian lineshape (FWHM =5.5 eV) which satisfactorily reproduces the leading edge of the 20 K spectrum, apart from a possible weak shoulder at 877 eV. The $\underline{c}f^1$ lineshape, obtained by subtraction, is also nearly Gaussian, with a broader tail at high transferred energy. The same lineshapes yield a good fit to the 300 K spectrum, only adjusting their relative intensities. If the $\underline{c}f^2$ peak were the result of a $2p^6 4f^1 \rightarrow 2p^5 4f^2 \rightarrow 2p^6 3d^9 4f^2$ E2 transition, we would expect its intensity to *decrease* in the α-phase, as a consequence of the smaller $4f^1$ weight in the initial state. On the contrary, the $I(f^2)/I(f^1)$ intensity ratio *increases* from 0.6 at 300 K to 0.9 at 20 K, reflecting the larger $4f^2$ weight in the hybrid ground state of α-Ce. There-
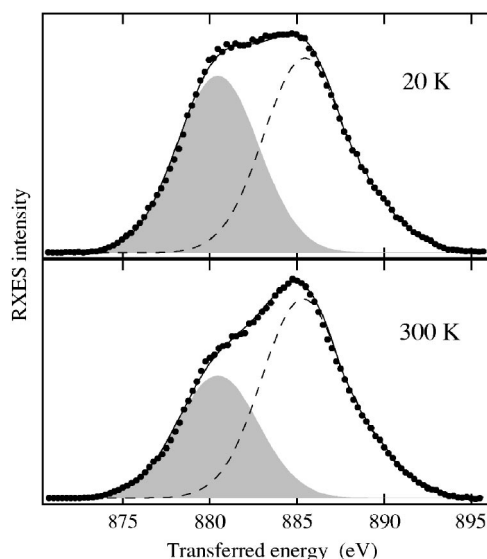

FIG. 5. Lα RXES spectra of Sc:Ce measured in the α (20 K) and γ (300 K) phases, after subtraction of the same linear background. The excitation energy corresponds to the maximum of the $\underline{c}f^2$ feature in the L$_3$ XAS of Fig. 1. The shaded areas and dashed curves represent the estimated $\underline{c}f^2$ and $\underline{c}f^1$ contributions.

fore, even if we cannot exclude a small E2 contribution, the pre-edge $\underline{c}f^2$ feature, and by the same argument the pre-edge XAS feature (Fig. 1), must be assigned to a predominantly dipolar transition. We notice that, in both phases, the relative weight of the f^2 RXES peaks is notably larger than the estimated ground state weight of the f^2 configuration (1–2%, Ref. 41), confirming the ability of RXES to enhance the contribution of a specific configuration by an appropriate choice of the excitation energy.

The observed variation reflects the larger f^2 weight in α-Ce. Hybridization in the RXES intermediate and final states reduces the f^2 and increases the f^1 contributions (the f^0 configuration is too far in energy to mix in), and reduces the intensity of a $|\Psi_0\rangle \rightarrow \underline{c}f^2$ transition. Our estimate is therefore a lower limit for the relative increase of the ground state f^2 term across the γ-α transition. It can be compared with the 100% increase derived from photoemission data in Ref. 41, which required a more elaborate analysis to separate surface and bulk signals.

In a schematic two-level description of a Ce impurity, and neglecting for simplicity the small $4f^2$ contribution, hybridization of the $4f^1$ and $4f^0 k$ configurations yields the ground state $|\Psi_0\rangle \sim \lambda|4f^1\rangle + \mu|4f^0 k\rangle$, of predominantly $4f^1$ character, and the mainly $4f^0$ excited state $|\Psi_{exc}\rangle \sim \lambda|4f^0 k\rangle + \mu|4f^1\rangle$. These are—schematically—also the final states of a RXES process. From the initial ground state, scattering may be *elastic* ($h\nu_T$=0), if the final state coincides with $|\Psi_0\rangle$, or inelastic ($h\nu_{OUT} < h\nu_{IN}$ or $h\nu_T > 0$) if the final state is the excited state $|\Psi_{exc}\rangle$. These processes are *neutral* and no core hole is present in the final state. Therefore RXES provides information on the hybrid ground state which is complementary to XAS, photoemission or Lα RXES.[42]

The "unpolarized" spectra of Fig. 6 are the sum of spectra measured with two distinct polarizations of the incident beam: perpendicular to (*vertical* polarization, V) or within
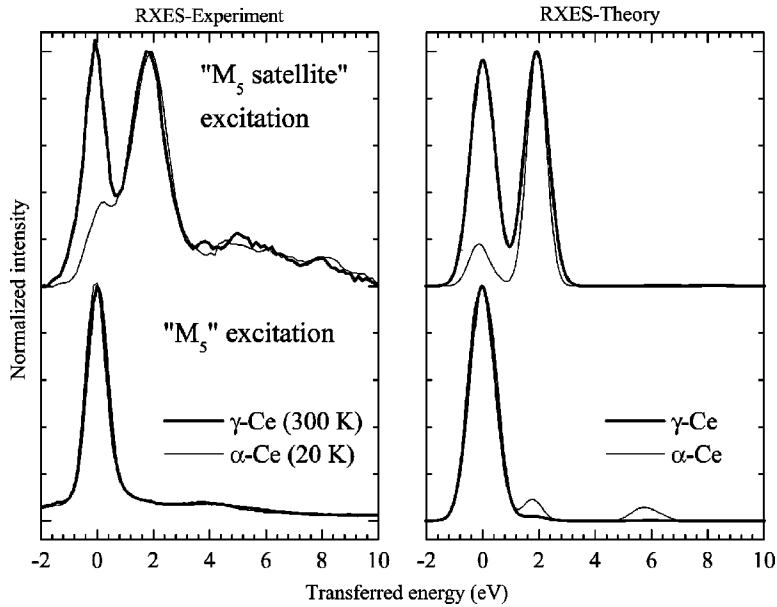
FIG. 6. Left: M_5 RXES spectra measured at 300 K and 20 K, at the maximum of the M_5 XAS profile (bottom) and at the f^1 satellite (top). The spectra were normalized to their background. Right: the corresponding spectra calculated within the cluster model: (i) α-Ce: $\varepsilon_f=-0.9$ eV; $V=0.23$ eV; $U_{ff}=7.0$ eV; (ii) γ-Ce: $\varepsilon_f=-1.4$ eV; $V=0.15$ eV; $U_{ff}=8.0$ eV. The elastic peak is at zero energy transfer.

(*horizontal* polarization, H) the horizontal scattering plane. Polarization effects are discussed below. The excitation energies coincide with the maximum of the M_5 XAS spectrum ($h\nu_{IN}=882$ eV, designated as "M_5" in the following), and with the f^1 satellite ($h\nu_{IN}=887$ eV). The spectra measured at M_5 are dominated by a peak at $h\nu_T=0$, from elastically scattered photons and possible unresolved low-energy excitations: we will refer to it for simplicity as the elastic peak. A much weaker inelastic tail corresponds to excited final states of f^0 (and f^2) character. The spectral lineshape is unaffected by the transition. Spectra measured in correspondence to the f^1 satellite exhibit, besides the elastic peak, a strong, broader peak centered at 2 eV, from the excited final states of mainly f^0 character. The relative intensity of the 2 eV feature and the elastic peak increases by ~ 4 times in the α phase. In the same figure we present theoretical spectra obtained by an AIM calculation, with transition probabilities described by the Kramers-Heisenberg formula. We adopted a cluster model with full multiplet effects, and restricted the basis states within three configurations, namely, $|(\underline{c})4f^0\rangle$, $|(\underline{c})4f^1k\rangle$, and $|(\underline{c})4f^2k^2\rangle$. The atomic Slater integrals and spin-orbit interaction parameters are obtained by Cowan's Hartree-Fock program with relativistic corrections,[43] and scaled as usual to 80% to account for intra-atomic configuration interaction and hybridization effects. We allowed the $4f$-band hybridization to be reduced by a factor $R_c(=0.6)$ in the presence of a core hole and enhanced by a factor $1/R_v$ ($R_v=0.9$) in the presence of an extra $4f$ electron.[44,45] The calculations are performed at $T=0$, which is not a serious limitation, because $T \ll T_K$ for α-Ce, and the $4f$ occupation of the thermally excited states ($n_f=1$) is close to that of the ground state in γ-Ce. The parameter values used are as follows: (i) for α-Ce $\varepsilon_f=-0.9$ eV (bare $4f$ energy), $U_{ff}=7.0$ eV (on-site Coulomb repulsion), $U_{fc}=10.5$ eV (core hole-$4f$ Coulomb interaction), $V=0.23$ eV (hybridization strength); (ii) for γ-Ce $\varepsilon_f=-1.4$ eV, $U_{ff}=8.0$ eV, $U_{fc}=10.5$ eV, $V=0.15$. Theory and experiment are in satisfactory agreement. At M_5 the dominant elastic peak is reproduced, even if the weak

feature at 2 eV is not observed in the experiment. At the f^1 satellite, the calculation correctly predicts the strong peak at 2 eV, and reproduces the large relative reduction of the elastic peak in the α phase. These spectral changes, which reflect the larger hybridization and associated f^0 weight in the ground state of the α phase, are enhanced at this specific excitation energy, which selects intermediate states of $\underline{c}f^1$ character.

The curves of Fig. 7, for excitation at the f^1 satellite, give an overall impression of the influence of the parameters on
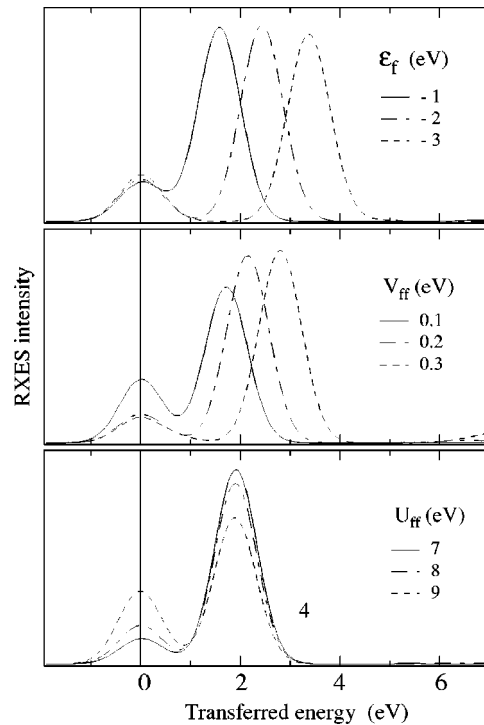

FIG. 7. Calculated M_5 RXES spectra for various values of the AIM parameters. Top: $V=0.25$ eV; $U_{ff}=8.0$ eV. Middle: $\varepsilon_f=-1.0$ eV; $U_{ff}=8.0$ eV. Bottom: $\varepsilon_f=-1.0$ eV; $V=0.25$ eV.
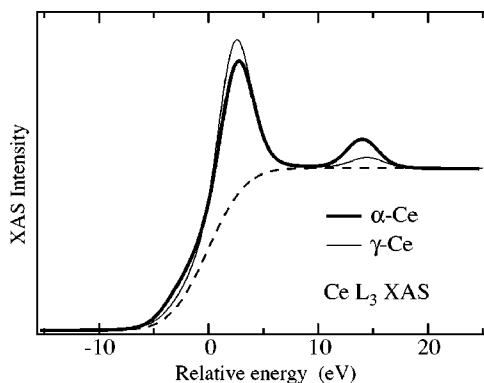
FIG. 8. Calculated Ce L_3 PFY-XAS spectra for α-Ce and γ-Ce. The AIM parameters are those used for the RXES calculation of Fig. 6. The step-like background accounts for transitions towards comtinuum states. Lifetime (Lorentzian, 0.4 eV) and experimental (Gaussian, 1.5 eV) broadenings have also been added.

FIG. 9. Calculated Ce $L\alpha$ RXES spectra for α-Ce, corresponding to incident energies indicated by solid symbols on the XAS profile (inset). All AIM parameters are the same as for Fig. 6.

the M_5 RXES spectral lineshape. The separation between the elastic and the f^0 peak increases, as expected, with $|\varepsilon_f|$, and with the hybridization V between the f^0 and f^1 configurations. The strength of the hybridization also influences their relative intensities. The Coulomb term U_{ff} has an indirect effect on the intensity of the f^0 peak through the relative weight of the f^0 and f^2 configurations in the initial and final states. In spite of the sensitivity of the calculated spectra to the AIM parameters, the experimental energy separation between the elastic peak and the satellite (Fig. 6) is essentially identical in the two phases. This is due to the combined effects of a *smaller* energy separation between the $4f^1$ and $4f^0k$ configurations, and a *larger* hybridization in α-Ce, which compensate for each other. In the schematic description outlined above, the energy separation between $|\Psi_0\rangle$ and $|\Psi_{exc}\rangle$ remains the same across the transition, even if the nature of these states is quite different in the two phases, as shown by the very different satellite intensities.

Figure 7 suggests that the choice of the AIM parameters is not unique: small changes in, e.g., ε_f could be compensated by appropriate changes in V to yield similar spectral lineshapes and n_f values. The variation of n_f between the two phases is the physical message of the AIM calculation. We obtain, respectively, $n_f=0.83$ for α-Ce and $n_f=0.94$ for γ-Ce, in excellent agreement with previous estimates from spectroscopic data.[35,41] These values are also consistent with the observed changes in the L_3 PFY-XAS spectrum of Fig. 1. In order to check the validity of our analysis, we used the same parameters to calculate L_3 PFY-XAS of the two phases (Fig. 8). After the addition of a rounded step-like background which simulates transitions to continuum states, and of an appropriate lifetime (Lorentzian, $\Delta E=0.4$ eV) and experimental (Gaussian, $\Delta E=1.5$ eV) broadenings, the calculated spectra reproduce the main features of the data, including the larger pre-edge shoulder in α-Ce. The sharper spectral shape of the calculated spectra with respect to the measured ones originates from the use of a cluster model, where the finite $5d$ band width is neglected. Similarly, the calculated $L\alpha$ RXES curves of Fig. 9 are in good agreement with the measured spectra of Fig. 4.

Finally, we consider the effect of the polarization of the incident radiation on the M_5 RXES. A strong linear dichro-
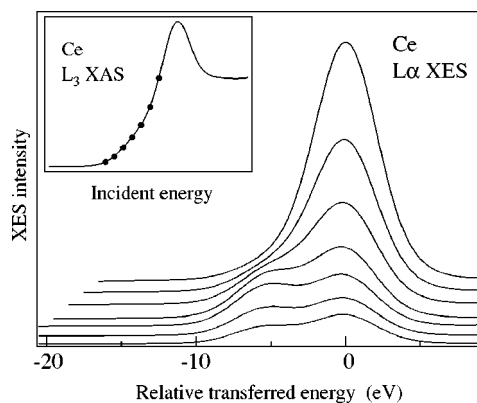
ism has been predicted[21] and later experimentally observed[22,23] in Ce compounds, when the electric field vector of the incident light is either perpendicular to ("polarized geometry") or lies within ("depolarized" geometry) the scattering plane. This effect is a direct consequence of the symmetry of the initial and final states and of the conservation of angular momentum: it does not require crystalline order or an anisotropic system. Theory predicts the suppression of the elastic peak in the depolarized geometry if the initial state is a singlet, i.e., for the "Kondo" ground state of a Ce impurity. Since the occupation of the singlet ground state depends on the ratio $(T/T_K)^{12}$, and T_K varies exponentially with the hy-
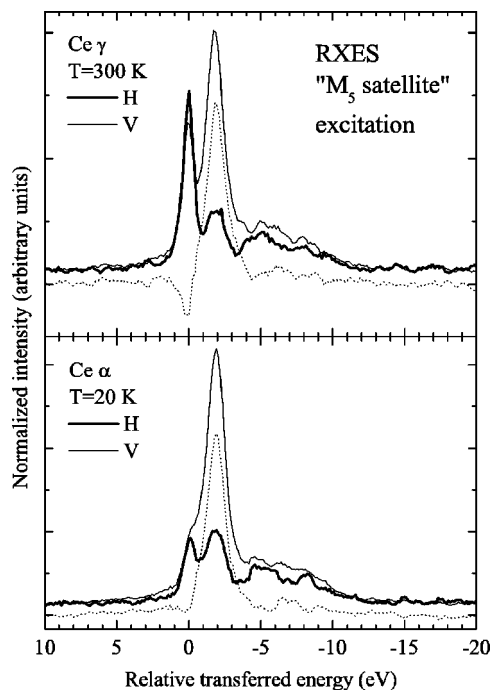

FIG. 10. Linear dichroism in the M_5 RXES spectra of Sc:Ce measured at the f^1 satellite. The electric field vector of the incident beam was either perpendicular to (V) or lying within (H) the horizontal scattering plane. The dotted curve is the difference (V−H).

bridization strength, the RXES dichroism is potentially a sensitive probe of hybridization in Ce materials. This is indeed confirmed by experiment.[22]

Polarization-dependent (H or V) Ce M_5 RXES spectra excited at the f^1 satellite are shown, for the two phases, in Fig. 10. In the notation of Ref. 31 our V geometry corresponds to ($\theta=90°$, $\phi=70°$) and is equivalent to the polarized geometry because the scattering cross section does not depend on ϕ, while H ($\theta=20°$, $\phi=0°$) is close but not identical to the depolarized ($\theta=0°$, $\phi=0°$) geometry. The spectra have been normalized to the intensity of the high energy tail, where we expect smaller polarization effects. In both phases we observe a large dichroism. The dichroism is especially large and positive on the peak at 2 eV energy transfer, consistent with the lower resolution spectra of Ref. 22 and with Ref. 23. On the elastic peak, on the other hand, the dichroism is essentially zero for α-Ce, and small but negative for γ-Ce, possibly suggesting that the "natural" normalization to the background that we adopted in Fig. 10 is not appropriate. Nevertheless, changes in the dichroism between the two phases remain meaningful. In particular, the integrated asymmetry ratio, i.e., $(V-H)/(V+H)$, over the whole spectrum was found in Ref. 22 to reflect hybridization in the ground state. We find that the integrated asymmetry ratio increases by more than 20% from 0.17 (300 K) to 0.21 (20 K), again in line with the larger hybridization in α-Ce.

IV. CONCLUSIONS

We utilized hard (L_3) and soft (M_5) x-ray absorption and resonant emission to revisit the α-γ transition in cerium. The present results not only confirm the changes in the $4f$ configuration deduced from previous spectroscopic data, but also add interesting elements for the interpretation of the spectral properties of intermediate-valence materials. In particular, thanks to the high resolution of PFY-XAS we could finally identify the missing f^2 feature predicted by theory in the L_3 absorption spectrum, and conclude that the local $4f$–$5d$ Coulomb repulsion is strongly reduced by metallic screening in bulk Ce. We determined a small but meaningful f^2 component in the hybrid ground state, and its change in the two phases, exploiting the possibility of selective enhancement of a specific electronic configuration in RXES. The emission dichroism, signature of the second-order nature of the process, offers additional information on the hybridization between localized and extended states and on their symmetry.

[1] A more sophisticated single-particle approach has been applied to evaluate the relative stability of various $4f$ configurations, see, e.g., Z. Szotek, W. M. Temmerman, and H. Winter, Phys. Rev. Lett. **72**, 1244 (1994).

[2] A. C. Hewson, *The Kondo Problem to Heavy Fermions* (Cambridge University Press, Cambridge, 1993).

[3] D. C. Koskenmaki and K. A. Gschneidner, Jr., *Handbook on the Physics and Chemistry of Rare Earths*, edited by K. A. Gschneidner, Jr. and L. Eyring (North-Holland, Amsterdam, 1978).

[4] R. Ramirez and L. M. Falicov, Phys. Rev. B **3**, 2425 (1971).

[5] B. Johansson, Philos. Mag. **30**, 469 (1974).

[6] J. W. Allen and R. M. Martin, Phys. Rev. Lett. **49**, 1106 (1982).

[7] M. B. Zölfl, I. A. Nekrasov, Th. Pruschke, V. I. Anisimov, and J. Keller, Phys. Rev. Lett. **87**, 276403 (2001).

[8] K. Held, A. K. McMahan, and R. T. Scalettar, Phys. Rev. Lett. **87**, 276404 (2001).

[9] J. W. Allen, S. J. Oh, O. Gunnarsson, K. Schönhammer, M. B. Maple, M. S. Torikachvili, and I. Lindau, Adv. Phys. **35**, 275 (1986).

[10] D. Malterre, M. Grioni, and Y. Baer, Adv. Phys. **45**, 299 (1996).

[11] O. Gunnarsson and K. Schönhammer, Phys. Rev. B **28**, 4315 (1983).

[12] N. E. Bickers, D. L. Cox, and J. W. Wilkins, Phys. Rev. B **36**, 2036 (1987).

[13] E. Weschke, C. Laubschat, T. Simmons, M. Domke, O. Strebel, and G. Kaindl, Phys. Rev. B **44**, 8304 (1991).

[14] L. Duò, S. De Rossi, P. Vavassori, F. Ciccacci, G. L. Olcese, G. Chiaia, and I. Lindau, Phys. Rev. B **54**, R17 363 (1996).

[15] A. Sekiyama, T. Iwasaki, K. Matsuda, Y. Saitoh, Y. Onuki, and S. Suga, Nature (London) **403**, 396 (2000).

[16] See, e.g., R. I. R. Blyth, J. J. Joyce, A. J. Arko, P. C. Canfield, A. B. Andrews, Z. Fisk, J. D. Thompson, R. J. Bartlett, P. Riseborough, J. Tang, and J. M. Lawrence, Phys. Rev. B **48**, 9497 (1993).

[17] L. Braicovich, M. Taguchi, F. Borgatti, G. Ghiringhelli, A. Tagliaferri, N. B. Brookes, T. Uozumi, and A. Kotani, Phys. Rev. B **63**, 245115 (2001).

[18] M. Taguchi, L. Braicovich, F. Borgatti, G. Ghiringhelli, A. Tagliaferri, N. B. Brookes, T. Uozumi, and A. Kotani, Phys. Rev. B **63**, 245114 (2001).

[19] C. Dallera, M. Grioni, A. Shukla, G. Vankò, J. L. Sarrao, J. P. Rueff, and D. L. Cox, Phys. Rev. Lett. **88**, 196403 (2002).

[20] S. M. Butorin, D. C. Mancini, J.-H. Guo, N. Wassdahl, J. Nordgren, M. Nakazawa, S. Tanaka, T. Uozumi, A. Kotani, Y. Ma, K. E. Myano, B. A. Karlin, and D. K. Shuh, Phys. Rev. Lett. **77**, 574 (1996).

[21] M. Nakazawa, H. Ogasawara, and A. Kotani, J. Phys. Soc. Jpn. **69**, 4071 (2000).

[22] C. Dallera, M. Marcon, G. Ghiringhelli, A. Tagliaferri, N. B. Brookes, G. Olcese A. Palenzona, and L. Braicovich, Solid State Commun. **121**, 635 (2002).

[23] M. Watanabe, Y. Harada, M. Nakazawa, Y. Ishiwata, R. Eguchi, T. Takeuchi, A. Kotani, and S. Shin, Surf. Rev. Lett. **9**, 983 (2002).

[24] K. A. Gschneidner, Jr., R. O. Elliot, and R. R. McDonald, J. Phys. Chem. Solids **23**, 1191 (1962).

[25] C. Dallera, E. Puppin, A. Fasana, G. Trezzi, N. Incorvaia, L.

Braicovich, N. B. Brookes, and J. B. Goedkoop, J. Synchrotron Radiat. **3**, 231 (1996).

[26] G. Ghiringhelli, A. Tagliaferri, L. Braicovich, and N. B. Brookes, Rev. Sci. Instrum. **69**, 1610 (1998).

[27] K. Hämäläinen, D. P. Siddons, J. B. Hastings, and L. E. Berman, Phys. Rev. Lett. **67**, 2850 (1991).

[28] S. Tanaka, K. Okada, and A. Kotani, J. Phys. Soc. Jpn. **63**, 2780 (1994).

[29] P. Carra, M. Fabrizio, and B. T. Thole, Phys. Rev. Lett. **74**, 3700 (1995).

[30] P. W. Loeffen, R. F. Pettifer, S. Müllender, M. A. van Veenendaal, J. Röhler, and D. S. Silvia, Phys. Rev. B **54**, 14 877 (1996).

[31] M. Nakazawa, K. Fukui, H. Ogasawara, A. Kotani, and C. F. Hague, Phys. Rev. B **66**, 113104 (2002).

[32] A. Kotani, T. Jo, and J. C. Parlebas, Adv. Phys. **37**, 37 (1988).

[33] D. Malterre, Phys. Rev. B **43**, 1391 (1991).

[34] B. Lengeler, G. Materlik, and J. E. Müller, Phys. Rev. B **28**, 2276 (1983).

[35] E. Wuilloud, H. R. Moser, W. D. Schneider, and Y. Baer, Phys. Rev. B **28**, 7354 (1983).

[36] B. T. Thole, G. van der Laan, J. C. Fuggle, G. A. Sawatzky, R. C. Karnatak, and J.-M. Esteva, Phys. Rev. B **32**, 5107 (1985).

[37] A. Kotani and S. Shin, Rev. Mod. Phys. **73**, 203 (2001).

[38] G. van der Laan, B. T. Thole, G. A. Sawatzky, J. C. Fuggle, R. Karnatak, J.-M. Esteva, and B. Lengeler, J. Phys. C **19**, 817 (1986).

[39] J.-M. Mariot, J.-J. Gallet, L. Journel, C. F. Hague, W. Felsch, G. Krill, M. Sacchi, J.-P. Kappler, A. Rogalev, and J. Goulon, Physica B **259-261**, 1136 (1999).

[40] L. Journel *et al.*, Phys. Rev. B **66**, 045106 (2002).

[41] L. Z. Liu, J. W. Allen, O. Gunnarsson, N. E. Christensen, and O. K. Andersen, Phys. Rev. B **45**, 8934 (1992).

[42] S. M. Butorin, D. C. Mancini, J.-H. Guo, N. Wassdahl, and J. Nordgren, J. Alloys Compd. **225**, 230 (1995).

[43] R. D. Cowan, *The Theory of Atomic Spectra* (University of California Press, Berkeley, CA, 1981).

[44] O. Gunnarsson and O. Jepsen, Phys. Rev. B **38**, 3568 (1988).

[45] K. Okada and A. Kotani, J. Electron Spectrosc. Relat. Phenom. **71**, R1 (1995).

[46] J.-P. Rueff *et al.*, Phys. Rev. Lett. **93**, 067402 (2004).